Nanoscale Res Lett (2010) 5:1456–1463
DOI 10.1007/s11671-010-9661-7

NANO EXPRESS

# Nanogrids and Beehive-Like Nanostructures Formed by Plasma Etching the Self-Organized SiGe Islands

**Yuan-Ming Chang · Sheng-Rui Jian · Jenh-Yih Juang**

Received: 19 April 2010 / Accepted: 25 May 2010 / Published online: 8 June 2010


**Abstract** A lithography-free method for fabricating the nanogrids and quasi-beehive nanostructures on Si substrates is developed. It combines sequential treatments of thermal annealing with reactive ion etching (RIE) on SiGe thin films grown on (100)-Si substrates. The SiGe thin films deposited by ultrahigh vacuum chemical vapor deposition form self-assembled nanoislands via the strain-induced surface roughening (Asaro-Tiller-Grinfeld instability) during thermal annealing, which, in turn, serve as patterned sacrifice regions for subsequent RIE process carried out for fabricating nanogrids and beehive-like nanostructures on Si substrates. The scanning electron microscopy and atomic force microscopy observations confirmed that the resultant pattern of the obtained structures can be manipulated by tuning the treatment conditions, suggesting an interesting alternative route of producing self-organized nanostructures.

**Keywords** SiGe · High-resolution reciprocal space mapping · SEM · AFM · TEM

## Introduction

Periodical nanostructures are of great research interest because of their potential applications in data storage [1–3] as well as in preparing photonic crystals [4, 5]. In order to realize such opportunities, the development of lithography techniques that are capable of fabricating large area periodical nanostructures with reasonable control over their size and periodicity is required. In general, two approaches, namely the top–down and the bottom–up, have been coined to label the techniques used to generate nanometer-sized structures. The conventional lithographical methods, including electron-beam lithography [6], photolithography [7] and focused ion beam lithography [8], are the representative top–down approaches widely implemented in manufacturing nano-scale semiconductor devices as well as nanostructures for various materials. However, these techniques often require very high capital investment and involve multiple-step processes, which not only limits the facility accessibility but also results in relatively high operation cost.

On the other hand, self-organized growth [9–11] has been demonstrated to be a viable bottom–up method for fabricating large area nanostructures with reasonable control of size and shape distributions. These structures can be, in turn, used as templates for building nanometer-scale structures. Here, we report a simple fabrication technique capable of producing large area, well-ordered, periodic nanogrids with sufficient size control in the sub-500-nm region. The present method consists of two major steps. First, the SiGe films deposited on Si substrates by ultrahigh vacuum chemical vapor deposition (UHVCVD) were transformed into self-assembled SiGe nanoisland arrays by thermal annealing. Second, the resultant SiGe nano-island arrays after subjected to subsequent reactive ion etching (RIE) treatments were found to result in either the quasi-beehive nanostructures or the self-organized nano-grids (SONGs) on Si substrates, depending on the conditions of RIE processes. It is noted that the current fabrication

Y.-M. Chang · S.-R. Jian (✉)
Department of Materials Science and Engineering,
I-Shou University, Kaohsiung 840, Taiwan
e-mail: srjian@gmail.com

J.-Y. Juang
Department of Electrophysics, National Chiao Tung University,
Hsinchu 300, Taiwan

method is advantageous in several respects. First, since the SiGe thin films were deposited in the UHVCVD system, hence the issue of contamination during the annealing process can be largely minimized. Moreover, owing to the fact that no aqueous chemical solution and metallic material were used in the manufacturing procedures, protection of the RIE system from major pollution sources is guaranteed. Finally, the lithography-less anisotropic etching process can reduce the fabrication cost significantly.

## Experimental Details

Figure 1 displays schematically the experimental procedures carried out in this work for fabricating the quasi-beehive Si nanostructures. Briefly, prior to the growth of SiGe thin film, the surface of Si substrate was cleaned by the standard Radio Corporation of America (RCA) procedures [12]. The Si wafers were then dipped in dilute hydrofluoric acid to form a passive surface layer, which allowed the wafers to maintain their clean surfaces when transported through air before being introduced into the loadlock chamber of the ultrahigh vacuum chemical vapor deposition (UHVCVD, ANELVA SRE-612 Japan) system [13, 14]. When the temperature reached 550°C and the deposition chamber was pumped to $1.2 \times 10^{-9}$ Torr using a turbo molecular pump, the wafers were transferred directly into the deposition chamber from the loadlock chamber. The inlet gas was a mixture of $Si_2H_4$ (flow rate: 1 sccm) and $GeH_4$ (flow rate: 7 sccm). The SiGe epitaxial thin films were grown on the p-type Si (100) substrate at a growth rate of $\sim$8 nm/min with a total thickness of about 100 nm (Fig. 1a) [15].

Following the film growth, in situ thermal annealing was carried out at 900°C for 30 min in the UHVCVD chamber to form the well-ordered SiGe nanoislands, as illustrated schematically in Fig. 1b. The annealed SiGe/Si assembles were then placed into the reactive ion etching (RIE, TEL TE5000 Japan) chamber and, subjected to RIE using $CF_4$ (40 sccm) and argon (200 sccm) at an RF power of 200 W for 3, 5, or 10 min, respectively, as depicted in Fig. 1c. The effect of ion bombardment was primarily determined by the ion energy, which, in turn, was dependent on the RF power and the self-bias. During the RIE process, when the reactive ions passed through the sheath region, the positive ions were accelerated under the inserted electric field to produce the ion bombardment effect that, in turn, etches the target materials to form the quasi-beehive Si nanostructures and the SONGs, as shown in Fig. 1d.

The high-resolution cross-sectional transmission electron microscopy (XTEM) image of thin film was analyzed with an operating voltage of 200 kV. The composition of the films was analyzed by Auger electron spectroscopy

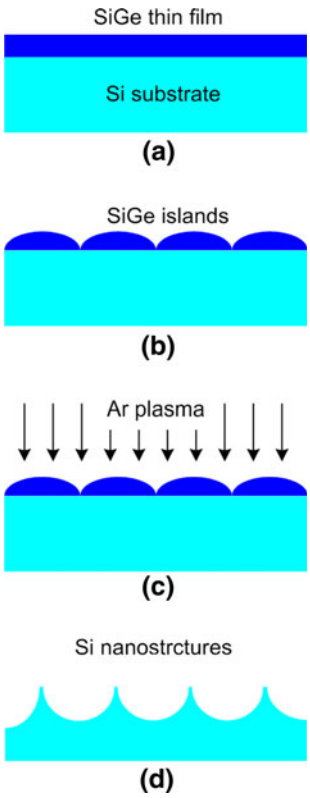


**Fig. 1** Fabrication procedures of quasi-beehive Si nanostructures and self-organized nanogrids: **a** SiGe thin film is deposited on Si substrate; **b** SiGe islands arrays are formed via the annealing treatment; **c** then plasma etching (RIE); **d** finally the self-organized nanostructures are fabricated

(AES, VG Scientific Microlab 310F). The Auger analyses were performed in a Physical Electronics-650 scanning Auger microprobe with a background pressure of $1.0 \times 10^{-9}$ Torr. High-resolution X-ray diffraction was used to determine the phase formation and crystallographic structure of all samples. High-resolution reciprocal space mapping (HRRSM) was applied to observe the structural features of SiGe thin films. The characteristics of the surface morphology of the Si substrate as well as that of the SiGe films were observed by field-emission scanning electron microscopy (FESEM). Atomic force microscopy (AFM) was also used to image the surface morphologies of the fabricated samples.

## Results and Discussion

A XTEM image of the as-grown SiGe thin film is displayed in Fig. 2. From the XTEM observation, the interface of SiGe/Si is atomically smooth and flat with no sign of existence of any misfit dislocations, indicating the completely coherent epitaxial relations between the film and substrate. In addition, the AES results displayed in the inset

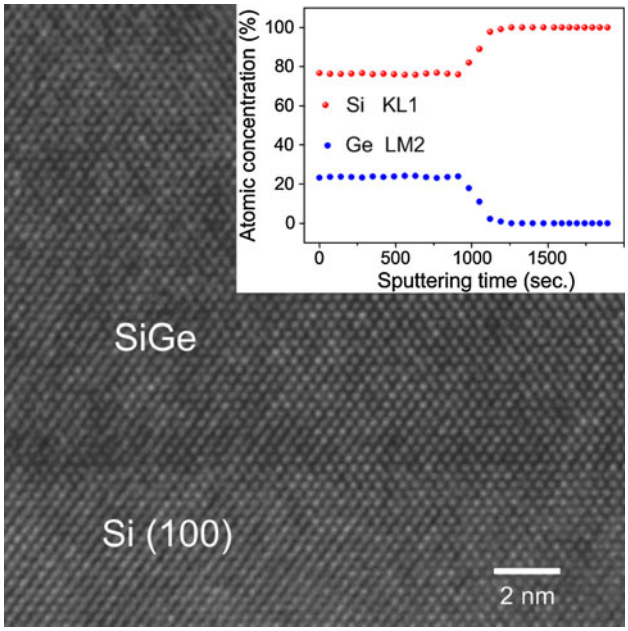


**Fig. 2** The cross-sectional HRTEM image of SiGe/Si sample prior to thermal annealing. *Inset* compositions of Si and Ge elements are confirmed by Auger analysis

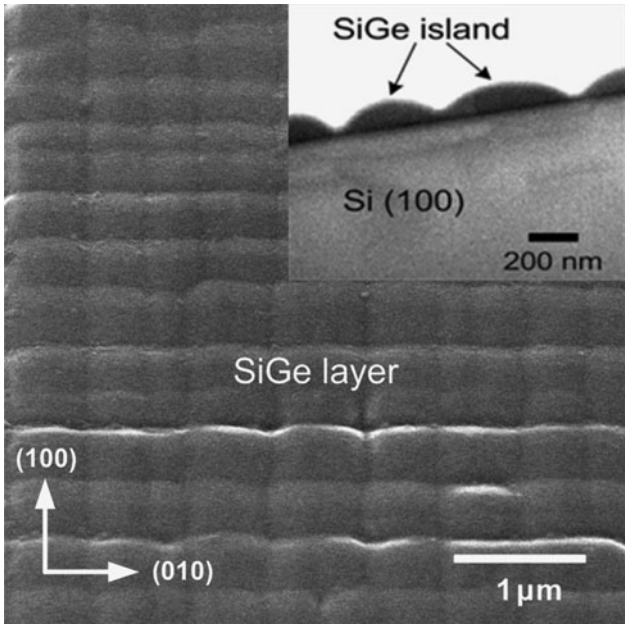


**Fig. 3** SEM observation the surface morphological image of SiGe thin film at an annealing temperature of 900°C. *Inset* the XTEM image of SiGe nanoislands on Si substrate

of Fig. 2 reveal that the Ge concentration is distributed uniformly throughout the film on Si substrates. The averaged Ge composition of the as-grown SiGe thin film was estimated to be around 24.4%. It is surprising that, in the present study, the apparent pseudomorphic growth of the dislocation-free SiGe strained layer can maintain to a much larger critical thickness than those reported previously [16, 17]. It is believed that the relative low growth temperature might have played a significant role. As will be described in more detail below, the strain relaxation and accompanied surface roughening induced by subsequent thermal annealing exhibited in the current films also displayed marked differences comparing to those reported by Timbrell et al. [16] and Ozkan et al. [17], where generation of dislocations and accompanied orientation change in surface roughening morphologies were evidently observed.

Figure 3 shows the typical top-view image observed by FESEM for SiGe films annealed at 900°C for 30 min. It is clear that the high temperature annealing-induced surface roughening has resulted in the formation of SiGe island grids along the (100) and (010) directions. The cross-sectional image of SiGe islands observed by XTEM displayed in the inset of Fig. 3 further indicates that in the vicinity of the interface between the SiGe islands and Si substrate remains essentially free of relaxation dislocations during the annealing process. Thus, the underlying mechanisms leading to the present observations certainly require further discussion. We first note that, unlike those reported by Xie et al. [18] where the Ge islands have been deliberately manipulated to nucleate on the intersections of misfit dislocation networks generated at the interface of an underneath SiGe strain layer and Si substrate, the formation of the present SiGe island array must have arisen from very different mechanisms. On the other hand, Floro et al. have demonstrated that heteroepitaxial stress between the SiGe layer and Si substrate cannot only result in coherent islanding of SiGe layer [19] but also have played the primary role in island shape transitions [20]. However, we note that the abovementioned reports were all derived based on observations performed during deposition, and the islanding of the SiGe layer may behave differently from that results from the post-deposition annealing. Indeed, as pointed out by Jesson et al. [21] that, in the case of annealed $Si_xGe_{1-x}$ films, especially at high supersaturations, the strain-induced roughening can bypass faceting and result in a transition with characteristics of the Asaro-Tiller-Grinfeld (ATG) instability [22, 23]. Within the context of the ATG instability, the strain field-induced surface roughening of semiconductor films is manifested by the appearance of continuous ripple morphology as displayed in Fig. 3. The reason for this is that the $Si_xGe_{1-x}$ film is under compressive strain with $\varepsilon \sim -0.04\ (1-x)$ [24] such that an undulation in the surface allows lattice planes to relax toward the ripple peaks. This lowers the elastic energy stored in the strained film but, at the same time, increases the surface energy relative to the planar layer. The competition between these two factors, in turn, gives rise to a condition for a minimum undulation length

scale $\lambda_c$ for which the morphology is stable. Here, $\lambda_c$ can be expressed as following:

$$\lambda_c = 2\pi\mu\gamma/(1-\nu)\sigma^2 \quad (1)$$

with $\mu$, $\gamma$, $\nu$, and $\sigma$ being the shear modulus, the surface energy density, the Poisson's ratio of the SiGe layer, and the misfit stress, respectively. Taking $\mu \sim 40$ GPa [21], $\gamma \sim 1$ J/m$^2$ [21], $\nu \sim 0.25$,[1] and $\sigma \sim 1.4$ GPa [19] one obtains a $\lambda_c \sim 170$ nm, which is much smaller than the averaged island spacing displayed in the inset of Fig. 3 (~400–500 nm) and those reported in Ref. [17] (~600 nm). Therefore, the obtained morphology can be indeed explained by the strain-induced roughening governed by the mechanism of ATG instability.

As has been pointed out by Jesson et al. [21], since there is no energy barrier to roughening except for mass transport along the surface, one of the consequences of the ATG instability-induced islanding is the formation of cusp. In order to elucidate this effect, Fig. 4 shows the relationship of the depth of self-organized nanoislands as a function of the annealing temperature for a fixed annealing time of 30 min. In this analysis, areas of $20 \times 20$ μm$^2$ of the annealed SiGe thin films are measured at various annealing temperatures. Based on these shape analyses, there are only sparsely distributed convex structures on the surface of the as-grown SiGe film. Even at the annealing temperature of 700°C, there are only few convex structures observed, indicating that at temperatures lower than 700°C the strain-induced roughening is hindered by either the lack of supersaturation or insufficient time for adequate mass transport. Nevertheless, as the annealing temperature is above 800°C the measured depth of the SiGe islands increases rapidly and reaches an average height of ~100 nm at 900°C, as shown in the inset of Fig. 4. In this case, the cusp feature is evidently displayed in the inset of Fig. 3 with the average depth being about the original film thickness. At this stage, we believe that film must have relaxed most of its strain.

In order to obtain a more quantitative measure on the evolution of the structural quality upon annealing, we chose the asymmetric (113)-reflection and the symmetric (004)-reflection HRRSM to compare the characteristics of the crystallographic structure of the as-grown SiGe sample with the one annealed at 900°C for 30 min. Figs. 5a, b reveal typical HRRSM around the asymmetric (113) reflections of the as-grown SiGe sample and the annealed sample, respectively. The HRRSM images are plotted on a logarithmic scale as a function of the reciprocal lattice

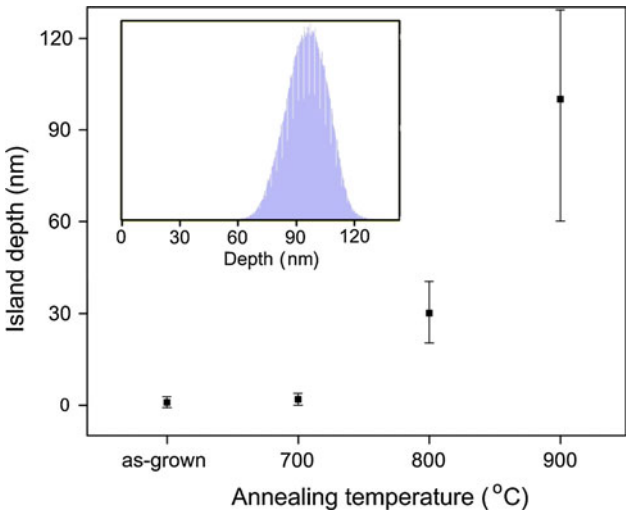


**Fig. 4** The depth of the self-organized nanoislands as a function of the annealing temperature. *Inset* the shape analysis of SiGe thin film with the annealing treatment at 900°C

vector parallel ($Q_x$) and perpendicular ($Q_y$) to the surface. From Fig. 5a, it is clear that the scattering distributions of the Si substrate and that of the SiGe thin film are in perfect alignment, indicating that the SiGe thin film is completely commensurate with the Si substrate. Moreover, the scattering distributions of the SiGe film and substrate are very narrow, indicative of the high crystalline quality and the low defect density in the as-grown SiGe film. On the other hand, Fig. 5b indicates that, after annealing at 900°C for 30 min, the scattering distributions of both SiGe film and Si substrate broadened in two directions, suggesting that significant degradation in crystallinity may have occurred in both of the SiGe film and Si substrate. This is consistent with the characteristics of ATG instability where the cusp regions are under tremendous compressive strain and the transported mass is rapidly accumulated at the island tips. The former is expected to have effects on the substrate, while the latter is certainly detrimental to the crystallinity of the resultant islands. This can be further confirmed by the HRTEM images displayed in Fig. 6, where the apparent degradation in the crystalline structure of the annealed SiGe islands (Fig. 6b) is clearly demonstrated by comparing that with the as-deposited one (Fig. 6a). It is also noted that the center of the scattering distribution of the SiGe film moves toward that of the Si substrate, indicating that the annealing processes has been accompanied by significant strain relaxation. Based on the current HRRSM analyses, the as-grown SiGe sample is apparently fully strained, and about 36% of the strain has been relaxed by annealing the sample at 900°C for 30 min.

Being inspired by defective structure revealed in the HRRSM analyses presented in Fig. 5, we have further tried

[1] Various values (ranging from 0.22 [23] to 0.28 [15]) of the Poisson's ratio for $Si_xGe_{1-x}$ films have been reported. Here, we take an average value for estimation only.

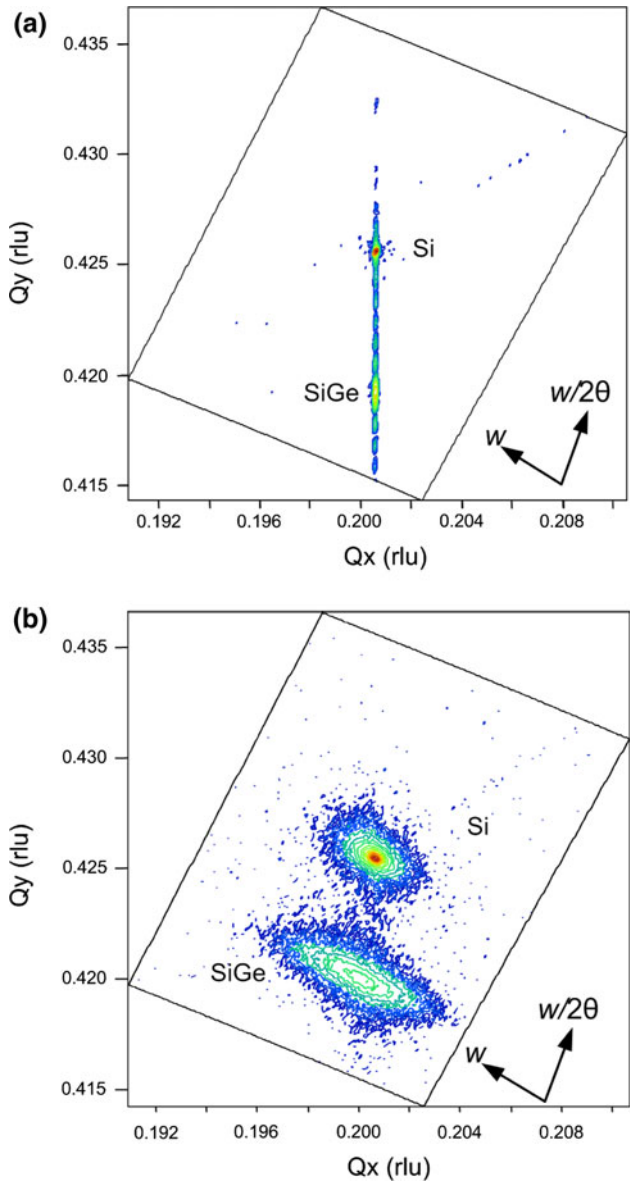


**Fig. 5** Asymmetric (113) HRRSM of **a** the as-grown SiGe thin film and, **b** the annealed SiGe thin film at 900°C for 30 min

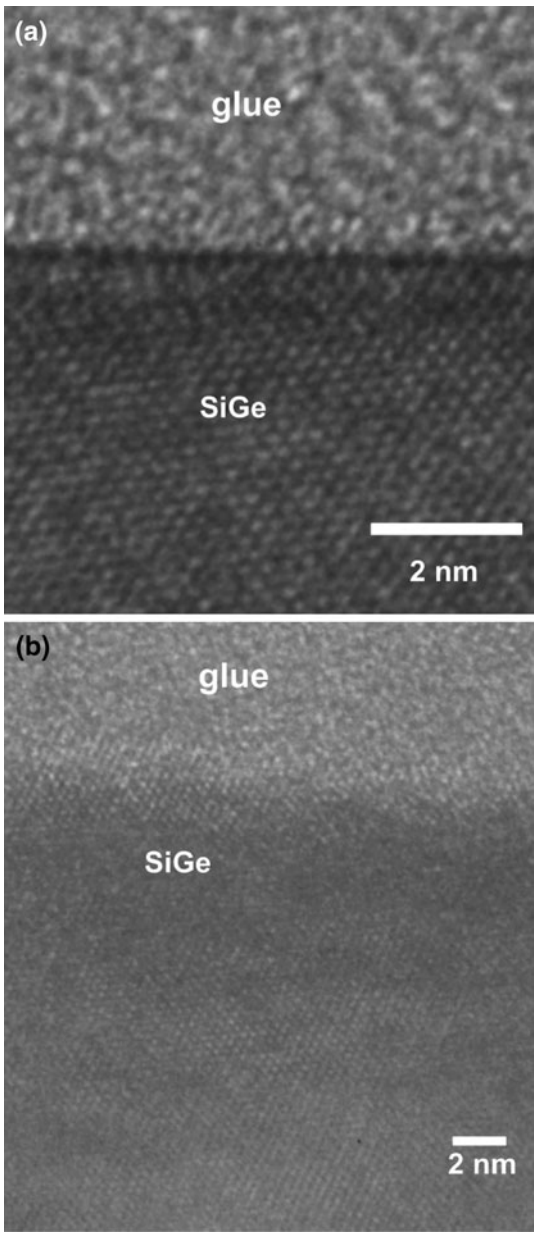


**Fig. 6** The HRTEM images of the **a** as-grown SiGe film and **b** SiGe film annealed at 900°C for 30 min. The results clearly indicate the degradation of crystalline structure resulted from the ATG instability-induced surface roughening driven by strain relaxation

to use the annealed sample as the template for creating various self-organized nanostructures. Fig. 7 presents one of the examples we have tried. The series of the SEM images shown in Fig. 7 display the surface morphology of the as-grown SiGe sample (Fig. 7a) and that of samples being first annealed at 900°C for 30 min followed by RIE etching with $CF_4$ gas for 3, 5, and 10 min (Fig. 7b, d), respectively. The surface morphology of as-grown SiGe sample is very smooth with a surface roughness of $\sim$0.32 nm over a $20 \times 20\ \mu m^2$ area (Fig. 7a). After annealing at 900°C (30 min) and RIE for 3 min, small cavities are evidently generated (Fig. 7b), which more or less following the island morphology shown in Fig. 3. Note here that, when compared with the AFM image shown in Fig. 7f for the same sample, in the SEM images displayed in Fig. 7b, e the regions with the convex dome shape appearance are in fact cavities while the light curvy lines are the ridges of the cavities. This is also consistent with the results reported by Oehrlein et al. [25]. In their studies, the etching rate of $Si_{0.8}Ge_{0.2}$ is more than two times faster than that of pure Si when using $CF_4$ as the primary RIE gas. In fact, it is generally conceived [26] that Ge is normally more susceptible to fluorine and, as a result, higher amount of fluoride (from $CF_4$ gas) often results in higher chemical etching probability and more severe depredation in the

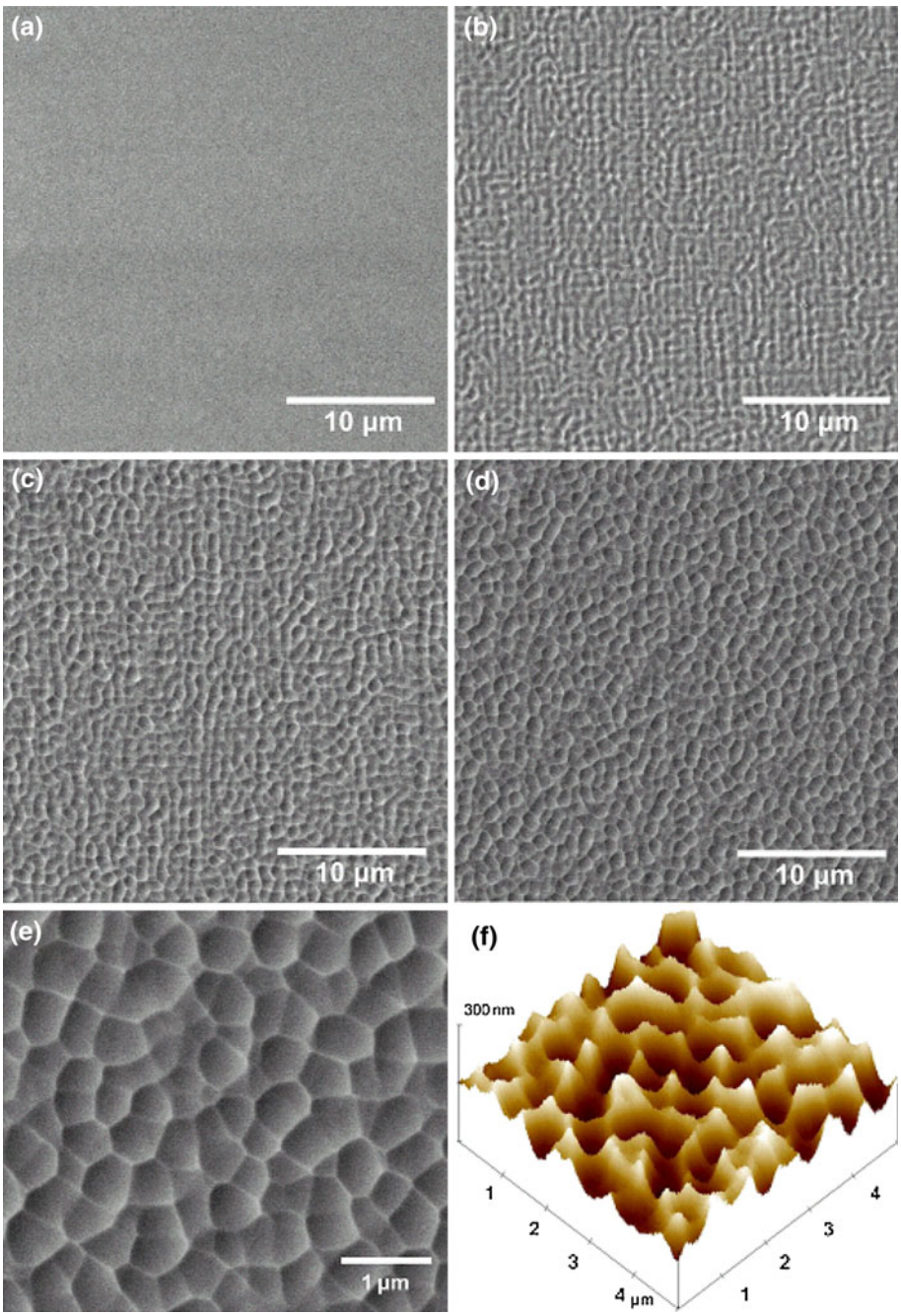


**Fig. 7** SEM *top-view* images of SiGe thin films with **a** as-grown sample, **b** 900°C annealed and 1 min RIE, **c** 900°C annealed and 5 min RIE, and **d** 900°C annealed and 10 min RIE. **e** The SEM and **f** AFM image of the quasi-beehive Si nanostructures

original structural arrangements. In any case, Fig. 7 evidently displays that with the increasing RIE time the nano-cavities grow bigger and deeper and finally form a quasi-beehive surface structure on the Si substrate. The results indicate that the amount and size of cavities and, hence, the details of the quasi-beehive structure can be closely monitored by controlling the RIE time.

To fully realize the application potential, we have further tried to develop methods of creating the nanostructures with more regular spatial arrangements. To this respect, instead of using the etching gases commonly used in the RIE system, we changed to use Ar plasma treatment on the annealed island array. To our surprise, even with as short as 1 min of Ar Plasma treatment, the highly concentrated and regularly distributed nanogrids consisting of nano-cavities and nano-tapers are clearly visible on Si substrate, as shown in Fig. 8a, c, d. The average diameter, height, and density of the nanocavities were $\sim$400–600 nm, $\sim$50–80 nm, and $\sim$3–4 $\mu m^{-2}$, respectively. With a slight increase of Ar plasma treatment to 3 min, a significant larger scale of nano-grids is obtained (Fig. 8b). It is noted that Ar plasma treatment not only is very efficient in

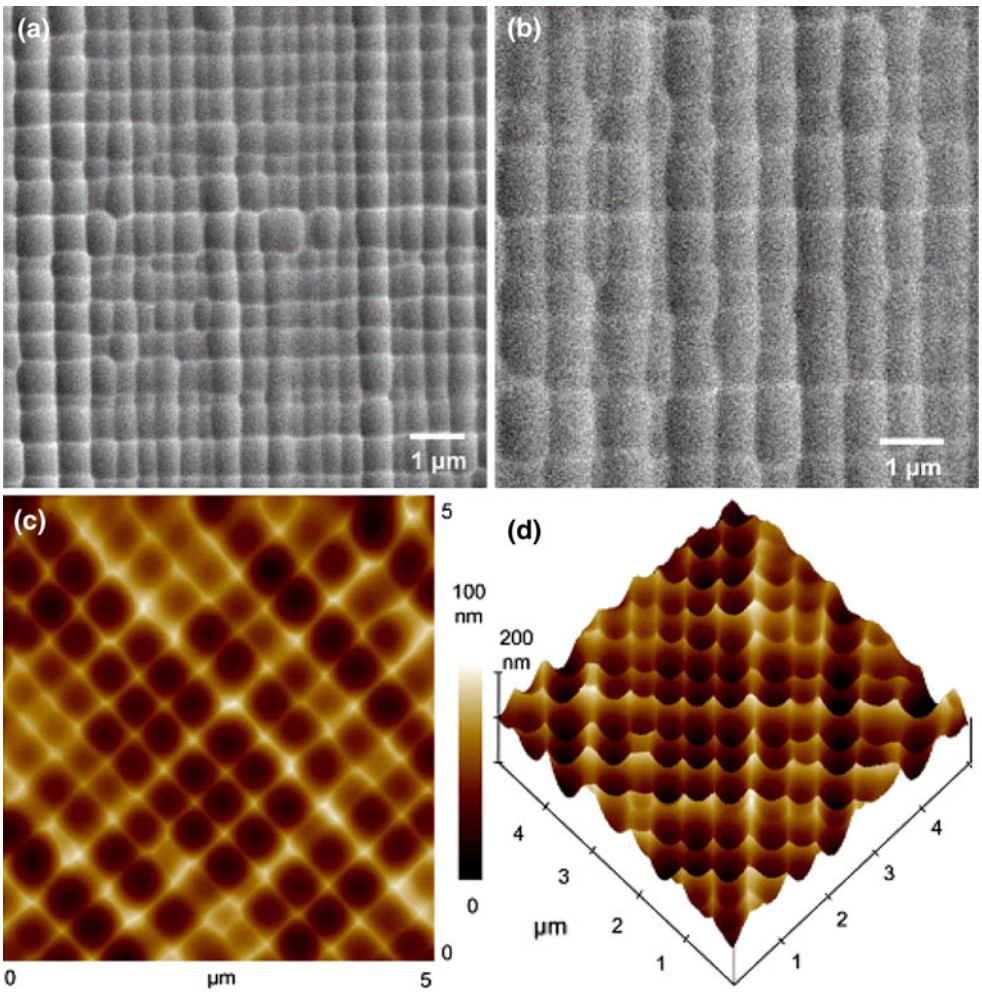


**Fig. 8** SEM *top-view* images of SiGe thin films with **a** 900°C annealed and 1 min Ar plasma, **b** 900°C annealed and 3 min Ar plasma. **c** 2-D and **d** 3-D AFM images of the self-organized nanogrids (**a**)

removing the defective self-organized SiGe islands formed after annealed at high temperatures but also is capable of maintaining the original self-organized patterns to later stages treatment. It is not clear at present why Ar plasma treatment can make such a dramatic difference when compared to that treated by more traditional RIE processes. Presumably, since Ar plasma etching is a more physical mean and no complicated chemical reactions are involved, the etching is more isotropic and is easier to maintain the original structural arrangements.

In any case, the present study has not only presented a detailed account for the formation of the self-organized nanoislands arrays by thermal annealing, but also has indicated a very efficient method of producing the much desired self-organized nano-grids (SONGs) on Si substrate by using the self-organized nanoisland arrays as the "sacrificing" mask. We emphasize that the present process has completely avoided the usage of any lithographic process, which should be of significant practical importance in future applications. Experiments using these SONGs nanostructure as the template substrate to fabricate nanostructures of various interesting materials are underway.

## Conclusion

In summary, we have shown that it is possible to fabricate self-organized nanogrids arrays on Si substrate by simply combining the thermal annealing and RIE (or Ar plasma) processes on the SiGe layers grown on Si substrate. The compositions and structures of SiGe thin film are characterized by using Auger and XTEM techniques to reveal island formation mechanism. The results indicate that the self-organized SiGe islands were formed via the Asaro-Tiller-Grinfeld instability-induced surface roughening driven by the strain established between the heteroepitaxy SiGe film and the Si substrate. A well-ordered self-organized nanogrids structure formed on the Si substrate was successfully demonstrated by treating the annealed SiGe film in Ar plasma for as short as only 1 min and without resorting to any lithographical means.

**Acknowledgments** This work was partially supported by the National Science Council of Taiwan, under Grant No.: NSC 97-2112-M-214-002-MY2. JYJ is supported in part by the National Science Council of Taiwan and the MOE-ATP program operated at NCTU. The authors would like to thank Prof. Ching-Liang Dai (Department of Mechanical Engineering, National Chung Hsing University, Taiwan) and Dr. Jiann Shieh and Hung-Min Chen (National Nano Device Laboratories, Taiwan) for their useful discussions. Assistances from Fu-Kuo Hsueh for UHVCVD, Chiung-Chih Hsu for TEM, Jie-Yi Yao for XRD and Chih-Ming Wu for RIE technical supports in National Nano Device Laboratories are also gratefully acknowledged.



## References

1. J.Y. Cheng, C.A. Ross, V.Z. Chan, H.E.L. Thomas, R.G.H. Lammertink, G.J. Vancso, Adv. Mater. **13**, 1174 (2001)
2. S. Yoshida, T. Ono, M. Esashi, Nanotechnology **19**, 475302 (2008)
3. X. Liu, M. Stamm, Nanoscale Res. Lett. **4**, 459 (2009)
4. S.M. Yang, G.A. Ozin, Chem. Commun. **24**, 2507 (2000)
5. M. Miyake, Y.C. Chen, P.V. Braun, P. Wiltzius, Adv. Mater. **21**, 3012 (2009)
6. J. Fujita, Y. Ohnishi, Y. Ochiai, S. Matsui, Appl. Phys. Lett. **68**, 1297 (1996)
7. J.G. Goodberlet, Appl. Phys. Lett. **76**, 667 (2000)
8. N. Kawasegi, N. Morita, S. Yamada, N. Takano, T. Oyama, K. Ashida, S. Momota, J. Taniguchi, I. Miyamoto, H. Ofune, Nanotechnology **18**, 375302 (2007)
9. Y. Xia, B. Gates, Y. Yin, Y. Lu, Adv. Mater. **12**, 693 (2000)
10. Y.Z. Xie, V.P. Kunets, Z.M. Wang, V. Dorogan, Y.I. Mazur, J. Wu, G.J. Salamo, Nano Micro Lett. **1**, 1 (2009)
11. Z.M. Wang, K. Holmes, Y.I. Mazur, G.J. Salamo, Appl. Phys. Lett. **84**, 1931 (2004)
12. P.V. Zant, Microchip Fabrication. 5th edn, (McGraw-Hill, Boston, 2004), p 126
13. W.T. Lai, P.W. Li, Nanotechnology **18**, 145402 (2007)
14. D.J. Bell, T.E. Bauert, L. Zhang, L.X. Dong, Y. Sun, D. Grützmacher, B.J. Nelson, Nanotechnology **18**, 055304 (2007)
15. M. Huang, C.S. Ritz, B. Novakovic, D. Yu, Y. Zhang, F. Flack, D.E. Savage, P.G. Evans, I. Knezevic, F. Liu, M.G. Lagally, ACS Nano **3**, 721 (2009)
16. P.Y. Timbrell, J.M. Baribeau, D.J. Lockwood, J.P. McCaffrey, J. Appl. Phys. **67**, 6292 (1990)
17. C.S. Ozkan, W.D. Nix, H. Gao, Appl. Phys. Lett. **70**, 2247 (1997)
18. Y.H. Xie, S.B. Samavedam, M. Bulsara, T.A. Langdo, E.A. Fitzgerald, Appl. Phys. Lett. **71**, 3567 (1997)
19. J.A. Floro, E. Chason, R.D. Twesten, R.Q. Hwang, L.B. Freund, Phys. Rev. Lett. **79**, 3946 (1997)
20. J.A. Floro, G.A. Lucadamo, E. Chason, L.B. Freund, M. Sinclair, R.D. Twesten, R.Q. Hwang, Phys. Rev. Lett. **80**, 4717 (1998)
21. D.E. Jesson, K.M. Chen, S.J. Pennycook, T. Thundat, R.J. Warmack, J. Electron. Mater. **26**, 1039 (1997)
22. R.J. Asaro, W.A. Tiller, Metall. Trans. **3**, 1789 (1972)
23. M.A. Grinfeld, Sov. Phys. Dokl. **31**, 831 (1986)
24. H.T. Johnson, L.B. Freund, J. Appl. Phys. **81**, 6081 (1997)
25. G.S. Oehrlein, G.M.W. Kroesen, E. de Frésart, Y. Zhang, T.D. Bestwick, J. Vac. Sci. Technol. A **9**, 768 (1991)
26. Y. Zhang, G.S. Oehrlein, E. de Frésart, J. Vac. Sci. Technol. A **11**, 2492 (1993)